Atmos. Chem. Phys. Discuss., 11, 26867–26895, 2011
www.atmos-chem-phys-discuss.net/11/26867/2011/
doi:10.5194/acpd-11-26867-2011

Atmospheric Chemistry and Physics Discussions

The evolution of microphysical and optical properties of an A380 contrail in the vortex phase

J.-F. Gayet[1], V. Shcherbakov[1,2], C. Voigt[3,4], U. Schumann[3], D. Schäuble[3], P. Jessberger[3], A. Petzold[3], A. Minikin[3], H. Schlager[3], O. Dubovik[5], T. Lapyonok[5], M. Krämer[6], and M. Kübbeler[6,7]

[1]LaMP, UMR6016 CNRS – Université Blaise Pascal, Clermont-Ferrand, France
[2]LaMP, Institut Universitaire de Technologie de Montluçon, Montluçon, France
[3]Institut für Physik der Atmosphäre, Deutsches Zentrum für Luft- und Raumfahrt (DLR), Oberpfaffenhofen, Germany
[4]Institut für Physik der Atmosphäre, Johannes Gutenberg, Universität Mainz, Germany
[5]LOA, UMR8518 CNRS/Univ. des Sciences et Technologies de Lille, Villeneuve d'Ascq, France
[6]Inst. for Energy and Climate Research, IEK-7, Forschungszentrum Jülich, Jülich, Germany
[7]Institute of Atmospheric and Climate Science, ETH Zurich, Switzerland

Received: 24 June 2011 – Accepted: 19 September 2011 – Published: 28 September 2011

Correspondence to: J.-F. Gayet (j.f.gayet@opgc.univ-bpclermont.fr)

Published by Copernicus Publications on behalf of the European Geosciences Union.

Abstract

The contrail from a large-body A380 aircraft has extensively been probed in the vortex and early dispersion regime with in situ instruments to measure microphysical and optical properties of contrail ice particles on the DLR research aircraft Falcon. Concentrations up to 340 cm^{-3} of ice particles with diameters $d > 0.9\,\mu m$ and extinction coefficients up to 7.0 km^{-1} were measured inside the plume. Initially the primary vortices were sampled about 270 m below the A380 flight altitude at contrail ages of 70 to 120 s in ice subsaturated conditions, followed by measurements in the secondary wake with contrail ages of 120 to 220 s at conditions near ice saturation. In the primary vortices the mean effective diameter was 3.5 µm and the maximum ice water content (IWC) was 7.0 mg m^{-3} increasing with altitude and ice saturation in the secondary wake to 4.8 µm and 10.0 mg m^{-3}. The asymmetry parameter was found to decrease systematically with contrail age (and altitude) from 0.87 to 0.80 indicating that ice crystals become more and more aspherical during ice crystal growth. In addition, an inversion approach was used to retrieve the ice particle size distribution and the partitioning between spherical and aspherical particles. In the young primary vortex 100 % of the ice particles were of spherical shape, whereas partitioning coefficients of 68 % and 44 % were found in the more aged secondary wake. The extrapolation of our results to older contrails under similar meteorological conditions suggests that contrails with ages over 5 min may be dominated by aspherically-shaped ice particles typical for natural mid latitude cirrus.

1 Introduction

So far, only a few in situ observations of microphysical and optical properties of young contrails exist, particularly in the vortex phase. Ice crystals with effective diameters below 3.5 µm and number concentrations above 1000 cm^{-3} have been detected in contrails younger than 10 s (Petzold et al., 1997; Heymsfield et al., 1998; Baumgardner and

ACPD
11, 26867–26895, 2011

Gandrud, 1998). Voigt et al. (2010) measured ice crystals with effective diameters of 5.2 µm and number concentrations slightly above 100 cm^{-3} in the 1 to 2 min old contrail of a CRJ 2 aircraft. The integration over an extensive data set of 14 contrails from 9 different aircraft leads to effective diameters of 4.8 µm and concentrations near 100 cm^{-3} of sub-10 min old contrails (Voigt et al., 2011). Based on numerous in situ studies of the contrail transition to cirrus, Schröder et al. (2000) derived slightly larger ice particles (up to 5 µm) with number concentrations decreasing by dilution to less than 100 cm^{-3} within the first minutes of contrail evolution (see also Poellot et al., 1999). Febvre et al. (2009) showed that quasi-spherical ice particles with diameters smaller than 5 µm control the optical properties of the plume shortly after formation, while larger aspherical ice crystals govern the optical properties of 20 min old contrails. Similarly, extinction measurements in contrails are scarce. Sussmann and Gierens (1999) report Lidar extinction profiles with peak values of 3 to 70 km^{-1} in a 20 s old contrail. Extinctions near 1 km^{-1} are reported by Voigt et al., (2010, 2011) in less than 10 min old contrails based on calculations from ice crystal size distributions. Febvre et al. (2009) measured extinctions between 0.3 and 0.5 km^{-1} in sub-20 min old contrails. In summary, only few direct observations of ice crystal properties in the vortex phase exist (Petzold et al., 1997; Baumgardner and Gandrud, 1998; Schröder et al., 2000; Voigt et al., 2010, 2011). Yet, the vortex phase is important for contrail model initialization since it determines the pathway for further contrail evolution (Unterstrasser et al., 2008).

This paper presents detailed in situ observations of a contrail in the vortex regime emitted by a large-body A380 aircraft over Germany. The measurements were performed with instruments onboard the DLR research aircraft Falcon during the CONCERT (CONtrail and Cirrus ExperRimenT) campaign from 22 October to 20 November 2008 (Voigt et al., 2010; Jurkat et al., 2011). Here we focus on more than 700 s of observations in the 70 to 220 s old contrail from the A380 aircraft. Microphysical and optical particle properties of the primary vortices and the secondary wake are presented in Sect. 3. An inversion approach is used in Sect. 4 in order to interpret the optical properties in terms of the spherical/non-spherical ice particle partitioning. Closure

ACPD
11, 26867–26895, 2011

studies between different in situ instruments give solid arguments for the validation of our results.

2 Aircraft measurements

2.1 Contrail particle probes

During the CONCERT campaign, the DLR Falcon research aircraft was equipped with a set of instruments to measure microphysical particle properties and trace gas composition in the UTLS (Upper Troposphere/Lower Stratosphere) region. Voigt et al. (2010) provide a detailed description of the instruments installed on the aircraft. For more detail we refer to that study and we give here only a brief description of the instruments addressed below.

Four instruments were used to detect microphysical and optical properties of contrails and cirrus clouds: (1) the Polar Nephelometer (PN), (2) the Cloud Particle Imager (CPI), (3) the PMS 2D-C all operated by LaMP, and (4) the FSSP-300 operated by DLR. Thanks to the combination of these independent techniques, a description of particles within a range of diameters varying from a few micrometers (typically 0.5 µm) to 2 mm was possible. Since this study addresses the properties of a young contrail with ice particle diameters smaller than 20 µm, only data of the Polar Nephelometer and the FSSP-300 will be presented.

The Polar Nephelometer (Gayet et al., 1997) measures the scattering phase function of an ensemble of cloud particles (i.e. water droplets or ice crystals or a mixture of these particles ranging from less than 1 µm to about 1 mm diameter), which intersect a collimated laser beam ($\lambda = 804$ nm) near the focal point of a parabolic mirror. The sampling volume is determined by the sampling surface (10 mm long and 5 mm diameter beam) multiplied by the Falcon cruise speed of approximately 200 m s^{-1}, i.e. 1 l for the acquisition frequency of 10 Hz. Direct measurement of the scattering phase function allows particle types (water droplets or ice crystals) to be distinguished and calculation

ACPD
11, 26867–26895, 2011

of the optical parameters to be performed (extinction coefficient and asymmetry parameter, see Gayet et al., 2002). Non-absorbing ice particles randomly oriented in the sampling section are assumed in deriving bulk quantities. The accuracies of the extinction coefficient and asymmetry parameter determination are estimated to be within about 25 % and 4 % respectively (Gayet et al., 2002; Jourdan et al., 2010).

It is interesting to evaluate the sensitivity of the Polar Nephelometer measurements to the particle-shape deviation from a perfect sphere in view of the errors on the asymmetry parameter estimation. Mugnai and Wiscombe (1986) used a model of Chebyshev particles for the evaluation of the main differences in optical properties between spherical and aspherical particles. This model considers sphere deformation and waviness parameters in order to simulate different aspherical shapes. It was shown that for a particle having diameter of 4 µm (i.e. the size parameter is of about 15.7 for Polar Nephelometer's wavelength of 0.8 µm) and for a sphere deformation of $\Delta d = 0.1\, d$ (where d is the unperturbed-sphere diameter) the error of the asymmetry parameter estimation is about 4 %. This means that within the measurement errors on g, a sphere deformation of 10 % can not be detected by the Polar Nephelometer because the deformation effect is below the sensitivity of the measurements. The corresponding particles hereafter are called "quasi-spherical".

The FSSP-300 optical particle counter nominally measures particles from 0.3 to 20 µm diameter (Baumgardner et al., 1992). In order to minimize the Mie ambiguities related to the probe diameter response, the particles were grouped into size channels according to the shape information of the ice particles given from the Polar Nephelometer measurements. For quasi-spherical particles (i.e. having the asymmetry parameter >0.85) eight channels were rebinned giving a diameter range from 0.9 to 22.9 µm, whereas nine channels describe the diameter range from 0.9 to 19.5 µm for non-spherical particles (i.e. asymmetry parameter < 0.85). Mie calculations were used to derive the size bins for spherical ice particles. Size bins for non-spherical particles were defined from T-matrix calculations by Borrmann et al. (2000) assuming aspherical (i.e. rotationally symmetric ellipsoid) particles with an aspect ratio of 1:2 and adjusted

ACPD
11, 26867–26895, 2011

to the calibrated probe response of the specific FSSP-300 used during CONCERT. In both cases the particles are composed of pure ice with a refractive index of 1.31 + *i*0. A closure method was used in order to validate the proposed FSSP-300 size calibration by comparing the extinction coefficients derived from the Polar Nephelometer and the FSSP-300. The results show that particles with diameters below 0.9 µm can be neglected and contrail optical properties are controlled by larger particles.

For dense contrail encounters, FSSP-300 channels no. 30 and 31 were found to be overcounting while this was not the case for less dense cirrus encounters. Coincidence effects may explain this effect (Baumgardner et al., 1992) and therefore these channels were excluded from the data analysis. These effects and resulting instrumental implications will be discussed in a forthcoming paper. Summarizing, the ice particle number concentrations reported here relate to the diameter range from 0.9 to 18.0 µm and to 16.1 µm for ice spheres and aspherical ice particles, respectively.

According to Field et al. (2003) and Heymsfield (2007), the FSSP-300 and Polar Nephelometer measurements are not likely to be affected by ice crystal-shattering effects since the recorded ice particles are quite small (effective diameter of 4 µm , maximum particle diameter of 20 µm) The comparison of our contrail data to cirrus observations confirms this hypothesis (Schröder et al., 2000; Voigt et al., 2010).

2.2 Trace gas instruments

Measurements of water vapor inside and outside of ice clouds have been performed by two techniques: the high precision hygrometer FISH (Fast In situ Stratospheric Hygrometer) operated by FZ Jülich (Zöger et al., 1999; Schiller et al., 2008) and a CR-2 frost point hygrometer operated by DLR (Busen and Buck, 1995; Voigt et al., 2010; Schumann et al., 2011). The FISH instrument is based on the Lyman-α photofragment fluorescence technique with a measurement frequency of 1 Hz. The overall uncertainties in the water vapor mixing ratio is ±6 % and in the relative humidity over ice RH ice ±10 % mainly related to uncertainties in the temperature data. The ambient air temperature was measured with an accuracy of 0.5 K with a PT 100 Rosemount sensor.

ACPD
11, 26867–26895, 2011

The frost point hygrometer CR 2 (Buck Research Instruments) measures the temperature of a mirror carrying a thin frost layer held in equilibrium with the ambient water vapor. The detection limit of the frost point hygrometer is better than 2 µmol mol^{-1} at a pressure of 200 hPa for a time resolution of 2 s. Depending on water vapor gradients, the response time of the frost point hygrometer is in the order of few seconds to one minute. The uncertainty in the water vapor mixing ratio is ±8 % (Schumann et al., 2011). The uncertainty in RH ice also includes the temperature uncertainty and amounts to ±12 %. Both water vapor instruments use a backward facing inlet to exclude the sampling of ice crystals, thus sample water vapor.

The NO and NO_y measurements were performed using the chemiluminescence technique (Schlager et al., 1997). The technique has extensively been used before for the identification of contrails and for the detection of NO and NO_y in contrails and cirrus clouds (Ziereis et al., 2000; Voigt et al., 2006; Schäuble et al., 2009). Sample air passes through a backward facing inlet with a PFA tube sampling air outside the aircraft boundary layer. Inside the cabin, the sample air is split into the NO and NO_y channels of the instrument. In the NO_y channel the air first passes through a heated gold converter where the different NO_y compounds are reduced to NO using CO as catalyst. Subsequently the chemiluminescence reaction of NO with O_3 is detected. In young tropospheric aircraft plumes NO_y is mainly composed of NO and NO_2. The accuracy/precision of the NO and NO_y measurements are 7/10 % and 10/15 %, respectively (Ziereis et al., 2000). The data are recorded with a time resolution of 1 s. Here, we use the NO_y measurements for contrail identification.

3 Observations

The contrail observations were obtained on 19 November 2008 on a flight over Germany from Hamburg to Oberpfaffenhofen. The contrail was generated by a commercial A380 aircraft crossing over Germany at noon on its flight from London to Singapore. It was detected for 30 min from 12:10 to 12:40 UT at altitudes of 10 430 to 10 700 m, the

ACPD
11, 26867–26895, 2011

upper level indicating the flight altitude of the A380 aircraft. The meteorological situation over Germany on that day was influenced by a high pressure system located northwest of France over the Atlantic and a low pressure system over northern Scandinavia transporting cold and humid air into the upper troposphere over Germany. Thus on 19 November 2008 at noon, a cirrus region moved from the North over Germany. The optically thick A380 contrail was produced above this cirrus region and/or sandwiched in between cirrus regions as shown on the photo in Fig. 1 taken a few minutes before the contrail sampling. At the flight level of the A380 (10 700 m, 239 hPa, flight level 350), the temperature of −56.5 °C and RHi at ice saturation, the threshold temperature for contrail formation is −48.4 °C (±1.2 °C) fulfilling the Schmidt-Appleman criterion (Schumann, 1996) for contrail formation (assuming an overall efficiency of propulsion of 0.35 which could be relevant for A380 aircraft).

The flight strategy was the following: in collaboration with the German air traffic control (DFS), the Falcon pilots managed to track the contrail using visual navigation and the guidance of the air traffic controllers. The real-time indication of several measurements onboard the aircraft (NO/NO_y and CN data, as well as FSSP-300 and Polar Nephelometer counts) were used to confirm the contrail penetrations and therefore gave additional information to refine the flight altitude. The Falcon successfully flew inside the contrail for almost 20 min at a speed near 200 m s^{-1}, slightly lower than the A380 cruise speed, so that the observations were performed at contrail ages from about 70 to 220 s progressively. The contrail was entered from below, five profiles were initially flown in the contrail followed by an extensive measurement period in the upper contrail part, the secondary wake of the A380. A movie taken from the cockpit of the Falcon confirms the detection of the primary vortices initially clearly separated from secondary wake (vertical wake gap), which was mainly probed at older contrail stages. This feature is typical for twin/four engine aircraft and situations with scattered natural cirrus being present (see scenario 2 on Fig. 2 from Sussmann and Gierens, 1999). Indeed, broken thin cirrus clouds with low optical depth (relatively transparent from aircraft observations) were observed above the sampled contrail (see Fig. 1).

ACPD
11, 26867–26895, 2011

Figure 2 displays time-series of the altitude and the NO_y measurements along with the microphysical and optical parameters of ice crystals such as the concentration of particles with diameter above 0.9 µm (Conc1) and 2.5 µm (Conc3), respectively, with both derived from FSSP-300 data, the extinction coefficient (Ext) and the asymmetry parameter (g) from Polar Nephelometer (PN) data, and ice water content (IWC) and effective diameter (D_{eff}) derived from FSSP-300 data. The approximate time separation between the aircraft is also reported indicating the contrail age at the considered sampling time. We calculated the contrail age from the separation of the flight tracks of both aircraft including the wind speed. The shaded colors of the altitude time-series have been defined according to the contrail age in order to facilitate the discussion of the results represented on the next figure (Fig. 3).

The results show that the Falcon explored the contrail vertical structure five times from 10 450 m/−54.0 °C to 10 700 m/−56.5 °C (A380 cruise altitude) and thereafter remained near the 10 650 m level. The well-marked NO_y peaks (up to 51 nmol mol^{-1}), which are observed at the lower sampling levels, are a clear signature of the primary vortex as we will discuss below. These sequences surprisingly are not correlated with the particle concentration (Conc1); only the first NO_y peak at 12:15:40 UT correlates with the highest extinction value (7.0 km^{-1}). This may be explained by small-scale heterogeneities of the vortex properties, which could be of the same order as the horizontal distances of the probe mounting positions on the Falcon (5–10 m). Such heterogeneities in the primary vortices are very well illustrated on the Plate 1a by Sussmann (1999) which relates ground-based lidar observations in fresh B747-aircraft contrail. Nevertheless, we underscore that the FSSP-300 and Polar Nephelometer measurements are in a very good agreement on average. We will discuss now the vertical profiles of the contrail properties in order to assess the evolution in the vortex stage.

ACPD
11, 26867–26895, 2011

3.1 Vertical properties of the A380 contrail in the vortex regime

Figure 3a–h displays the vertical profiles of several parameters measured from the beginning of the observations (12:14:00 UT, 70 s contrail age) to 12:26:00 UT (220 s contrail age, see Fig. 2). As indicated above, the shaded colors of the data points give indication of the contrail age. Panel (a) shows the highest NO_y peak of up to 46 nmol mol^{-1} occurring at the lower sampling levels, and exhibits a sharp decrease of the NO_y mixing ratio with altitude with lower mean value of 6.4 nmol mol^{-1} at the upper levels because of dilution.

At lower levels, the observations address the primary vortices in the vortex regime of the contrail younger than 120 s (see also Fig. 2). The corresponding range of the primary vortex altitudes is identified in Fig. 3 by the shadowed area. The definition of this range is somewhat arbitrary, but it roughly corresponds (~ 100 m) to theoretical vortex scale (60–70 m) before the dispersion regime considering a wing span (b) of 80 m (i.e. $(4/\pi)$ b, see Unterstrasser et al., 2008). The relatively low NO_y mixing ratio and the measurement levels near the altitude of the contrail-forming aircraft (10 700 m) suggest that the measurements from 12:18:30 UT until 12:26:30 UT were performed in the secondary wake of the contrail (120–220 s aged), which remains above the sinking primary vortex.

The measurements at intermediate levels, identified by rather low NO_y mixing ratio values, i.e. above the primary vortex (~ 10 500 m) and below the secondary wake (~ 10 600 m) could be related to the buoyant cloudy plume, which is detrained upwards from the sinking vortex pair (see Fig. 3). Sussmann (1999) named this cloudy region "vertical wake-gap". For simplicity, we include the vertical wake-gap in our secondary vortex region. Our in situ measurements confirm that ice particles can be observed in the vertical wake-gap before the dispersion regime.

According to the altitude differences between the contrail top and bottom (~ 270 m) and to the corresponding contrail age (~ 110 s), a descent speed of 2.5 m s^{-1} is estimated for the vortex pair. This value roughly corresponds to the theoretical value of

ACPD
11, 26867–26895, 2011

$3\,m\,s^{-1}$ computed for an aircraft of similar mass (500×10^3 kg) and wingspan (80 m) as the A380 (Gerz et al., 2002).

Panels (b) and (c) of Fig. 3 represent the concentration measurements of ice particles larger than 0.9 µm and 2.5 µm, respectively. Conc1 and Conc3 reach $340\,cm^{-3}$ and $120\,cm^{-3}$ respectively. The large dispersion of the data points is explained by small scale heterogeneities of the plume as mentioned above. For instance, the transient peak of extinction ($7.0\,km^{-1}$) measured by the Polar Nephelometer in the primary vortex during a sequence of only 3 s (at 12:15:37 UT on Fig. 2, and seen at the 10 450 m level on Fig. 3d) is not correlated with the extinction derived from the FSSP-300. This instrument was likely out of the vortex, whereas the PN (mounted on the opposite wing) sampled the plume. Therefore the particle concentration and the ice water content on Fig. 3b, e are not representative for the primary vortex properties, which denotes the difficulties in determining average contrail properties from in situ measurements at very young contrail ages. Considering reliable values of extinction and effective diameter of $7.0\,km^{-1}$ and 3.5 µm, respectively (see Fig. 3d, f), the ice particle concentration and ice water content may be estimated in the primary vortex to $360\,cm^{-3}$ and $8\,mg\,m^{-3}$ according to the relationships given by Gayet et al. (2009). In conclusion, similar maximum values characterize all the contrail parts in terms of particle concentration, extinction coefficient and ice water content ($340–360\,cm^{-3}$, $5.0–7.0\,km^{-1}$, $7.4–10.0\,mg\,m^{-3}$, respectively). The effective diameter increases from 3.5 to 4.8 µm with altitude (Fig. 3f). In a few cases, the effective diameter approached 14 µm. Theses cases are likely caused by larger ice crystals embedded in the contrail, potentially from precipitation out of the thin scattered cirrus clouds observed above the A380 contrail (see Fig. 1). The large ice crystals were detected from both 2D-C and CPI instruments.

3.2 Interpretation of the observations

The asymmetry parameter information (from PN data) along with the microphysical properties discussed above and the identification of the wakes provide possibility to give the interpretation of the contrail vortex phases. We recall that large g-values

ACPD
11, 26867–26895, 2011

characterize spherical or quasi-spherical particles (>0.85 in our study). The smaller the g-values, the more aspherical the particles are (see e.g. Gayet et al., 2002; Mishchenko et al., 2002: their Fig. 10.14 for the size parameter >10). Note that the particles named "quasi-spherical" have been defined above (see Sect. 2.1).

Unlike microphysical properties presented above, the vertical profile of the asymmetry parameter, displayed on Fig. 3g, shows a rather smooth decrease with the altitude from 0.87 to 0.85–0.80. In the primary vortex (70–120 s aged) and prior the dispersion regime, spherical or quasi-spherical ice particles with diameter of 3.5 µm and a concentration of about 360 cm^{-3} control the optical properties of the contrail. Number concentrations of 1000 cm^{-3} of micrometer sized ice crystals have been reported by Petzold et al. (1997) and Schröder et al. (2000) for plume ages from <2 to 10 s. Baumgardner and Gandrud (1998) measured a few hundred particles by cm^{-3} in 10 s and 30 s old contrails. The downward movement associated with the vortex sinking (at a speed estimated to be of 2.5 m s^{-1}) leads to adiabatic heating and subsequent sublimation processes of the ice crystals (Lewellen and Lewellen, 2001). The humidity measurements of the Lyman-α and the frost point measurements displayed on Fig. 3h are near saturation in the secondary wake at the upper level of the contrail and decrease to 84 % in the lower part, the primary vortices. Hence the ice particles in the primary vortices (older than 70 s) were likely sublimating with the smallest measured size and the larger asymmetry parameter.

This brings up the question if ice sublimation processes can explain the observed spherical or quasi-spherical ice crystal shapes. Laboratory experiments (see for instance, Nelson, 1998) indicate that sublimating prismatic ice crystals evolve into confocal ellipses rotated about their major or minor axis (prolate or oblate spheroids). In situ measurements (Korolev and Isaac, 2004) show that ice particles during the final stage of evaporation are of quasi-spherical shape. Nevertheless, the observations referenced above report measurements of rather large sublimating ice crystals (i.e. larger than 100 µm), and from our knowledge no data are available to describe sublimation processes of very small ice crystals with diameters below 5 µm as those reported in

ACPD
11, 26867–26895, 2011

this study. Although we cannot rule out sublimation processes as potential sources for the observed effects, we may assume a primary quasi-spherical shape of the fresh ice particles as reported by Schröder et al. (2000) from replica images. Due to the limited set of data from our case study, we cannot exclude the possibility that the freshly quasi-spherical ice particles have first passed a transient growth regime (as long as RHi is supersaturated). Then according to our observations (i.e. for contrail older than 70 s), the ice particles are sublimating when they are downwards transported along with the primary vortices.

We highlighted that during the transition between the primary and the secondary vortices (sampled from 70 to 120 s aged), the asymmetry parameter smoothly decreases with the altitude from 0.87 to 0.85 (see Fig. 3g). This g-variation indicates that the ice particles are progressively loosing spherical shape and become more and more aspherical. In the next section, we will give a more detailed interpretation of this feature from inversion results. The particle shape behavior with the subsequent variation of the effective diameter profile (see Fig. 3f) may indicate that growing ice particles are found in the plume which is detrained upwards from the sinking vortex pair. As for other microphysical properties of this region, there are no significant differences with the characteristics of the primary wake in terms of maximum values of particle concentration, extinction and IWC (340 cm^{-3}, 6.6 km^{-1} and 7.4 $mg\,m^{-3}$ respectively). A detailed discussion and model simulations of contrails in a subsaturated environment can be found in an accompanying paper (Kübbeler et al., 2011).

The secondary wake aged from 120 to 220 s was sampled at a quasi-constant altitude near the A380 cruising altitude. During this 100 s of sampling, the asymmetry parameter decreased from 0.85 to 0.80 on average (see Fig. 2 and Fig. 3g with shaded colors). This feature illustrates very well the time-evolution of ice crystals towards more aspherical shapes and larger effective diameters (4.8 µm on average) indicating growing processes due to supersaturated RHi at this level The maximum values of particle concentration and extinction are of the same order as in other plume levels (350 cm^{-3} and 5.0 km^{-1} respectively) but larger IWC (up to 10 $mg\,m^{-3}$).

ACPD
11, 26867–26895, 2011

4 Spherical and aspherical ice particles partitioning in the A380 vortex phase contrail

In order to give a more detailed interpretation of the results, particularly regarding the shape of the ice particles, we used the approach, the inversion code, and the kernels look-up tables developed by Dubovik et al. (2006). It was demonstrated that these look-up tables of kernels allow usage of a mixture of spheroids of different aspect ratios and sizes as a generalized aerosol model (representing spherical, aspherical, and mixed aerosols) in remote sensing retrievals of atmospheric aerosols. Specifically, it offers the possibility to retrieve a complete set of aerosol parameters, including the complex refractive index and the size and shape distributions. This software is employed in operational processing of AERONET (AErosol RObotic NETwork) for retrieving detailed properties from observations of ground-based sun/sky-radiometers (Eck et al., 2008). In this work, the model was applied for the first time to the observations of ice particles of fresh contrail, i.e. with small diameters no larger than 20 µm or a size parameter no larger than 80 (for Polar Nephelometer's wavelength of 0.8 µm). It should be noted the original kernels generated by Dubovik et al. (2006) covered the range of the real part of the refractive index from 1.33 to 1.6. Therefore, in order to cover the properties of ice particles the kernels were extended down to 1.29.

To be specific, we modeled contrails as a mixture of two fractions, one is spherical and one is aspherical particles. Although ice particles are never ellipsoidal, we consider randomly oriented spheroids as a reasonable approximation of quite small aspherical particles. As for the axis ratio distribution of the aspherical fraction, we used a mixture of oblate and prolate spheroids with the modes at the values of 0.5 and 1.5, respectively.

Three representative examples of retrievals are discussed below. They were selected for contrail ages of 70, 105 and 205 s. The corresponding time-sequences A, B and C are identified in the time-series in Fig. 2 by shadowed areas. In Fig. 4a–c, the left panel displays the directly measured with FSSP-300 particle size distribution (solid

ACPD
11, 26867–26895, 2011

line) and the retrieved one (solid black circles). The size distribution was retrieved along with the refractive index $m = n + i\chi$ and the spherical/aspherical partitioning ratio (SAR) of ice particles. In the following, the SAR defines the percentage number of spherical particles relative to the total number of particles. Furthermore, the partitioning ratio is assumed to be constant over the full size range of the retrieved particle size distribution. Table 1 summarizes the results for each considered case. For all three cases, the real part of the refractive index was 1.31 ± 0.002. According to our retrievals, the particles were either nonabsorbing $\chi = 0$ or weakly absorbing with an upper bound for the imaginary part of $\chi \leq 10^{-4}$. Measurement errors mask the variations of phase functions when χ varies within the interval $[0; 10^{-4}]$ (Verhaege et al., 2008). As for the spherical/aspherical partitioning, it follows from our sensitiviy tests and simulations that the SAR value was larger than 98 % for the case A; the SAR estimation error was ±3 % for other cases.

The right panel of Fig. 4a–c represents the following data. The average scattering phase function (without normalization) measured by the Polar Nephelometer is shown by solid red circles. The FSSP phase function (blue plus-symbols) was calculated from the FSSP-300 size distribution assuming that all ice particles are spherical. The retrieved phase function shown by solid black circles was computed from the retrieved size distribution with consideration for the SAR. Both theoretical phase functions were computed for the refractive index $m = 1.31 + i\ 1.0 \times 10^{-4}$. We note in passing, that these curves can not be distinguished in the log-log scale from the phase functions computed for the refractive index of pure ice $m = 1.31 + i\ 1.3 \times 10^{-7}$ ($\lambda = 0.8\,\mu m$).

The main result of Fig. 4 is that the retrieved phase functions agree quite well with the observations from the Polar Nephelometer. This agreement is quantified with the residual values on Table 1 which are lower than 13.6 %. These errors are mainly due to uncertainties on the Polar Nephelometer measurements at backward scattering angles ($\theta > 150^{\circ}$, see Fig. 4). We recall that the residual (Res) are defined as follows:

ACPD
11, 26867–26895, 2011

$$\mathrm{Res} = 100\sqrt{\frac{1}{N}\sum_{i=1}^{N}\left[\frac{I_{\mathrm{ret}}(\theta_i) - I(\theta_i)_{\mathrm{meas}}}{I(\theta_i)_{\mathrm{meas}}}\right]^2} \quad (1)$$

where $I(\theta_i)$ is the phase-function value at the scattering angle θ_i, the subscripts "meas" and "ret" refer to the measured and retrieved values, respectively.

Likewise, compared to the direct observations the retrieved size distributions show roughly the same mode size and spreading for the cases A and B, whereas the retrieved size distribution exhibits a bimodal feature for the case C (Fig. 4c). In any case the modeled values of the extinction coefficient match quite well the measured one (see Table 1), highlighting quite robust results with respect to small variations of the observations.

Noteworthy results are found by interpreting the optical properties of the three contrail parts. In the primary vortex of the age of 70 s (Fig. 4a) all ice particles (100 %) are of quasi-spherical shape, which is supported by the close agreement of PN measurements and the theoretical FSSP-300 phase function (blue plus-symbols). This means that in the younger contrail part (70 s aged) spherical particles control the optical properties of the plume. Figure 4b addresses the properties of the contrail 105 s aged. The differences between the measured (PN) and theoretical (FSSP-300) phase functions at sideward scattering angles undoubtedly reveal the occurrence of non-spherical particles. Indeed the retrieved partitioning ratio of 68 % (see Table 1) indicates that 68 % of the ice particles are spherical and 32 % are aspherical. From these 32 % of aspherical particles one half is assumed oblate spheroids with an aspect ratio of 0.5 and the other half is assumed prolate spheroids with an aspect ratio of 1.5. In Fig. 4c, the differences between the phase functions (PN and FSSP-300) at sideward scattering angles are larger than in the previous case indicating a larger proportion of aspherical ice particles. This feature is confirmed by the retrieved partitioning ratio of 44 %. Therefore aspherical particles (28 % oblates and 28 % prolates) dominated the optical properties of the secondary wake contrail 205 s aged.

ACPD
11, 26867–26895, 2011

In order to summarize the results above, we have reported on Fig. 5 the relationships between the partitioning ratio (Fig. 5a) and the asymmetry parameter (Fig. 5b) versus the contrail age. Additional inversion results have been drawn on Fig. 5. Extrapolating the results on Fig. 5a, b, all ice particles could be aspherical-shaped after roughly 300 s assuming constant environmental conditions such as relative humidity, static air temperature, and dynamical properties like vertical wind velocity. The asymmetry parameter may then reach typical values for natural cirrus at mid-latitudes of 0.77 (Gayet et al., 2004). The g-value reported by Febvre et al. (2009) for a contrail 150 s aged fits quite well with our observations (see open circle on Fig. 5b).

It has to be noted that this study is based on 200 s of measurements in vortex-phase contrails which is a small subset of the 30 min contrail data collected in total behind the A380. Since the observed properties strongly depend on highly variable atmospheric thermodynamic and dynamic conditions, the reported results have to be taken as a case study without claiming general validity.

5 Conclusions

This paper presents first in situ measurements in the vortex stage of a contrail emitted by a large body A380 commercial aircraft. The observations covered the contrail vortex stage during its aging from 70 to 220 s.

The primary vortices were initially clearly separated from secondary wake (vertical wake gap), which was mainly probed at older contrail stages. This feature is typical for twin/four engine aircraft. The flight was proceeded to explore the contrail depth and gave possibility to perform unique measurements in the primary vortex (70–120 s aged) and the secondary vortex (120–220 s aged) in a range of temperature from −54.0 °C to −56.5 °C. The small scale heterogeneities of the vortex properties being of the order of the horizontal distances of the probe mounting positions on the Falcon (5–10 m) hampered the representativeness of the measurements and the derived mean contrail properties.

ACPD
11, 26867–26895, 2011

In the primary vortex (70–120 s aged) and prior the dispersion regime, spherical or quasi-spherical ice particles with diameter of 3.5 µm and a concentration of about 360 cm^{-3} control the optical properties of the contrail. High values of the extinction coefficient and ice water content were measured (7.0 km^{-1} and 8.0 mg m^{-3} respectively). The RHi values suggest subsaturation for which the ice particles in the primary wake were likely sublimating with subsequent smallest sizes and the larger asymmetry parameter (0.87).

The observations in the plume between the primary and the secondary wakes show a smooth decrease of the asymmetry parameter (0.87–0.85) versus the altitude (and time) indicating that the ice particles were progressively loosing their spherical shape and becoming more and more aspherical. This behavior may indicate that growing ice particles are found in the plume, which is detrained upwards from the sinking vortex pair, consistent with the variation of the effective diameter.

During the sampling of the secondary wake (120 to 220 s aged) at a quasi-constant level near the A380 cruising altitude, the asymmetry parameter decreased from 0.85 to 0.80 on average. This feature illustrates very well the time-evolution of ice crystals towards more aspherical shapes and larger effective diameters (4.8 µm on average) due to supersaturated RHi at this level. The maximum values of particle concentration and extinction are of the same order as in other plume levels (350 cm^{-3} and 5.0 km^{-1} respectively) but larger IWC (up to 10 mg m^{-3}).

A detailed interpretation of the results concerning the shape of the ice particles has been presented. We employed the approach, the code, and the kernels developed by Dubovik et al. (2006). The code along with the kernels offers the possibility to retrieve a complete set of ice particle parameters on the base of measured scattering phase functions (PN). The set of parameters includes the size distribution, the refractive index, and the spherical/aspherical ice particle partitioning. This technique, applied to the plume sampled at different ages (50, 105 and 205 s) gives quite robust results. In the primary vortex 70 s aged the ice particles (100 %) have all a quasi-spherical shape. Partitioning ratios of 68 % and 44 % are retrieved in the secondary vortex, 105 and 205 s aged,

ACPD
11, 26867–26895, 2011

respectively. This means that the proportion of spherical ice particles is decreasing with the contrail age in accordance with the subsequent decreasing of the asymmetry parameter. Extrapolating the results, ice particles could be all aspherically-shaped after roughly 300 s assuming constant environmental conditions such as relative humidity, static air temperature, and dynamical properties and the asymmetry parameter could reach typical values for natural cirrus at mid-latitudes.

Acknowledgements. The CONCERT campaign was organized by the HGF-junior research group AEROTROP (Impact of Aircraft Emissions on the heteROgeneous chemistry of the TROPopause region). Part of this work was funded within the DLR-project CATS (Climate-compatible Air Transport System) and by the DFG SPP HALO 1294. This work was funded by a grant from the CNRS/INSU. We thank the DLR flight department for extraordinary flights. We thank T. Hamburger for FSSP-300 instrument preparation. K. Gierens is thanked for helpful discussions. We thank C. Gourbeyre and J.-F. Fournol (LaMP) for their technical assistance. The Deutsche Lufthansa (A. Waibel) and the German air traffic control (DFS) are gratefully acknowledged for their excellent support of the campaign.

The publication of this article is financed by CNRS-INSU.

References

Baumgardner, D., Dye, J. E., Gandrup, B. W., and Knollenberg, R. G.: Interpretation of measurements made by the Forward Scattering Spectrometer Probe (FSSP-300) during the Airborne Arctic Stratosphere Expedition, J. Geophys. Res., 97, 8035–8046, doi:10.1029/91JD02728, 1992.

ACPD
11, 26867–26895, 2011

Baumgardner, D. and Gandrud, B. W.: A comparison of the microphysical and optical properties of particles in an aircraft contrail and mountain wave cloud, Geophys. Res. Lett., 25, 1129–1132, doi:10.1029/98GL00035, 1998.

Borrmann, S., Luo, B., and Mishchenko, M.: Application of the T-matrix method to the measurement of aspherical (ellipsoidal) particles with forward scattering optical particle counters, J. Aerosol Sci., 31, 789–799, doi:10.1016/S0021-8502(99)00563-7, 2000.

Busen, R. and Buck, A. L.: A high-performance hygrometer for aircraft use: Description, installation, and flight data, J. Atmos. Ocean. Tech., 12, 73–84, doi:10.1175/1520-0426(1995)012<0073:AHPHFA>2.0.CO;2, 1995.

Dubovik, O., Sinyuk, A., Lapyonok, T., Holben, B. N., Mishchenko, M., Yang, P., Eck, T. F., Volten, H., Muñoz, O., Veihelmann, B., van der Zande, W. J., Leon, J.-F., Sorokin, M., and Slutsker, I.: Application of spheroid models to account for aerosol particle nonsphericity in remote sensing of desert dust, J. Geophys. Res., 111, D11208, doi:10.1029/2005JD006619, 2006.

Eck, T. F., Holben, B. N., Reid, J. S., Sinyuk, A., Dubovik, O., Smirnov, A., Giles, D., O'Neill, N. T., Tsay, S.-C., Ji, Q., Al Mandoos, A., Ramzan Khan, M., Reid, E. A., Schafer, J. S., Sorokine, M., Newcomb, W., and Slutsker, I.: Spatial and temporal variability of column-integrated aerosol optical properties in the southern Arabian Gulf and United Arab Emirates in summer, J. Geophys. Res., 113, D01204, doi:10.1029/2007JD008944, 2008.

Febvre, G., Gayet, J.-F., Minikin, A., Schlager, H., Shcherbakov, V., Jourdan, O., Busen, R., Fiebig, M., Kärcher, B., and Schumann, U.: On optical and microphysical characteristics of contrails and cirrus, J. Geophys. Res., 114, D02204, doi:10.1029/2008JD010184, 2009.

Field, P. R., Wood, R., Brown, P. R. A., Kaye, P. H., Hirst, E., Greenaway, R., and Smith, J. A.: Ice particle interarrival times measured with a fast FSSP, J. Atmos. Ocean. Tech., 20, 249–261, doi:10.1175/1520-0426(2003)020<0249:IPITMW>2.0.CO;2, 2003.

Gayet, J. F., Crépel, O., Fournol, J. F., and Oshchepkov, S.: A new airborne polar Nephelometer for the measurements of optical and microphysical cloud properties. Part I: Theoretical design, Ann. Geophys., 15, 451–459, doi:10.1007/s00585-997-0451-1, 1997.

Gayet, J.-F., Asano, S., Yamazaki, A., Uchiyama, A., Sinyuk, A., Jourdan, O., and Auriol, F.: Two case studies of winter continental-type water and mixed-phase stratocumuli over the sea: 1. Microphysical and optical properties, J. Geophys. Res., 107, 4569, doi:10.1029/2001JD001106, 2002.

Gayet, J.-F., Ovarlez, J., Shcherbakov, V., Ström, J., Schumann, U., Minikin, A., Auriol, F.,

ACPD
11, 26867–26895, 2011

Petzold, A., and Monier, M.: Cirrus cloud microphysical and optical properties at southern and northern midlatitudes during the INCA experiment, J. Geophys. Res., 109, D20206, doi:10.1029/2004JD004803, 2004.
Gayet, J.-F., Treffeisen, R., Helbig, A., Bareiss, J., Matsuki, A., Herber, A., and Schwarzenboeck, A.: On the onset of the ice phase in boundary-layer Arctic clouds, J. Geophys. Res., 114, D19201, doi:10.1029/2008JD011348, 2009.
Gerz, T., Holzäpfel, F., and Daracq, D.: Commercial aircraft wake vortices, Prog. Aerosp. Sci., 38, 181–208, doi:10.1016/S0376-0421(02)00004-0, 2002.
Heymsfield, A. J.: On measurements of small ice particles in clouds, Geophys. Res. Lett., 34, L23812, doi:10.1029/2007GL030951, 2007.
Heymsfield, A. J., Lawson, P. R., and Sachse, G. W.: Growth of ice crystals in a precipitating contrail, Geophys. Res. Lett., 25, 1335–1338, doi:10.1029/98GL00189, 1998.
Jourdan, O., Mioche, G., Garret, T. J., Schwarzenbock, A., Vidot, J., Xie, Y., Shcherbakov, V., Duroure, C., Yang, P., and Gayet, J.-F.: Coupling of the microphysical and optical properties of arctic clouds during the ASTAR 2004 experiment: Implications for light scattering modelling, J. Geophys. Res., 115, D23206, doi:10.1029/2010JD014016, 2010.
Jurkat, T., Voigt, C., Arnold, F., Schlager, H., Kleffmann, J.,Aufmhoff, H., Schäuble, D., Schaefer, M., and Schumann, U.: Measurements of HONO, NO, NO_y and SO_2 in aircraft exhaust plumes at cruise, Geophys. Res. Lett., 8, 38, L10807, doi:10.1029/2011GL046884, 2011.
Korolev, A. and Isaac, G.: Observation of sublimating ice particles in clouds, Proc. 14th Int. Conf. on Clouds and Precipitation, ICCP2004, 19–23 July 2004, Bologna, Italy, 2004.
Kübbeler, M., Hildebrandt, M., Meyer, J., Schiller, C., Hamburger, Th., Jurkat, T., Minikin, A., Petzold, A., Rautenhaus, M., Schlager, H., Schumann, U., Voigt, C., Spichtinger, P., Gayet, J.-F., Gourbeyre, C., and Krämer, M.: Thin and subvisible cirrus and contrails in a subsaturated environment, Atmos. Chem. Phys., 11, 5853–5865, doi:10.5194/acp-11-5853-2011, 2011.
Lewellen, D. C. and Lewellen, W. S. : The effects of aircraft wake dynamics on contrail development, J. Atmos. Sci., 58, 390–406, 2001.
Mishchenko, M. I., Travis, L. D., and Lacis, A. A.: Scattering, Absorption, and Emission of Light by Small Particles, Cambridge University Press, Cambridge, 2002.
Mugnai, A. and Wiscombe, W. R.: Scattering from nonspherical Chebyshev particles, Part 1: Cross-sections, single-scattering albedo, asymmetry factor and backscatterd fration, Appl. Optics, 25, 1235–1244, doi:10.1364/AO.25.001235, 1986.

ACPD
11, 26867–26895, 2011

Nelson, N.: Sublimation of Ice Crystals, J. Atmos. Sci., 55, 910–919, doi:10.1175/1520-0469(1998)055<0910:SOIC>2.0.CO;2, 1998.
Petzold, A., Busen, R., Schröder, F. P., Baumann, R., Kuhn, M., Ström, J., Hagen D., Whitefield, P., Baumgardner, D., Arnold, F., Borrmann, S., and Schumann, U.: Near field measurements on contrail properties from fuels with different sulfur content, J. Geophys. Res., 103, 29867–29880, doi:10.1029/97JD02209, 1997.
Poellot, M., Arnott, W., and Hallett, J.: In situ observations of contrail microphysics and implications for their radiative impact, J. Geophys. Res., 104, 12077–12084, doi:10.1029/1999JD900109, 1999.
Schäuble, D., Voigt, C., Kärcher, B., Stock, P., Schlager, H., Krämer, M., Schiller, C., Bauer, R., Spelten, N., de Reus, M., Szakáll, M., Borrmann, S., Weers, U., and Peter, Th.: Airborne measurements of the nitric acid partitioning in persistent contrails, Atmos. Chem. Phys., 9, 8189–8197, doi:10.5194/acp-9-8189-2009, 2009.
Schiller, C., Krämer, M., Afchine, A., Spelten, N., and Sitnikov, N.: The ice water content in Arctic, midlatitude and tropical cirrus, J. Geophys. Res., 113, D24208, doi:10.1029/2008JD010342, 2008.
Schlager, H., Konopka, P., Schulte, P., Schumann, U., Ziereis, H., Arnold, F., Klemm, M., Hagen, D. E., Whitefield, P. D., and Ovarlez, J.: In situ observations of air traffic emission signatures in the North Atlantic flight corridor, J. Geophys. Res., 102, 10739–10750, doi:10.1029/96JD03748, 1997.
Schröder, F., Kärcher, B., Duroure, C., Ström, J., Petzold, A., Gayet, J.-F., Strauss B., Wendling, P., and Borrmann, S.: On the transition of contrails into cirrus clouds, J. Atmos. Sci., 57, 464–480, doi:10.1175/1520-0469(2000)057<0464:OTTOCI>2.0.CO;2, 2000.
Schumann, U.: On conditions for contrail formation from aircraft exhausts, Meteorol. Z., 5, 4–23, 1996.
Schumann, U., Weinzierl, B., Reitebuch, O., Schlager, H., Minikin, A., Forster, C., Baumann, R., Sailer, T., Graf, K., Mannstein, H., Voigt, C., Rahm, S., Simmet, R., Scheibe, M., Lichtenstern, M., Stock, P., Rüba, H., Schäuble, D., Tafferner, A., Rautenhaus, M., Gerz, T., Ziereis, H., Krautstrunk, M., Mallaun, C., Gayet, J.-F., Lieke, K., Kandler, K., Ebert, M., Weinbruch, S., Stohl, A., Gasteiger, J., Groß, S., Freudenthaler, V., Wiegner, M., Ansmann, A., Tesche, M., Olafsson, H., and Sturm, K.: Airborne observations of the Eyjafjalla volcano ash cloud over Europe during air space closure in April and May 2010, Atmos. Chem. Phys., 11, 2245–2279, doi:10.5194/acp-11-2245-2011, 2011.

ACPD
11, 26867–26895, 2011

Sussmann, R.: Vertical dispersion of an aircraft wake: Aerosol-lidar analysis of entrainment and detrainment in the vortex regime, J. Geophys. Res., 104, 2117–2129, doi:10.1029/1998JD200033, 1999.

Sussmann, R. and Gierens, K.: Lidar and numerical studies on the different evolution of vortex pair and secondary wake in young contrails, J. Geophys. Res., 104, 2131–2142, doi:10.1029/1998JD200034, 1999.

Unterstrasser, S., Gierens, K., and Spichtinger, P.: The evolution of contrail microphysics in the vortex phase, Meteorol. Z., 17, 145–156, 2008.

Verhaege, C., Shcherbakov, V., and Personne, P.: Limitations on retrieval of complex refractive index of spherical particles from scattering measurements, J. Quant. Sprectosc. RA., 109, 2338–2348, doi:10.1016/j.jqsrt.2008.05.009, 2008.

Voigt C., Schlager, H., Ziereis, H., Kärcher, B., Luo, B. P., Schiller, C., Krämer, M., Popp, P. J., Irie, H., and Kondo, Y.: Nitric acid in cirrus clouds, Geophys. Res. Lett., 33, L05803, doi:10.1029/2005GL025159, 2006.

Voigt, C., Schumann, U., Jurkat, T., Schäuble, D., Schlager, H., Petzold, A., Gayet, J.-F., Krämer, M., Schneider, J., Borrmann, S., Schmale, J., Jessberger, P., Hamburger, T., Lichtenstern, M., Scheibe, M., Gourbeyre, C., Meyer, J., Kübbeler, M., Frey, W., Kalesse, H., Butler, T., Lawrence, M. G., Holzäpfel, F., Arnold, F., Wendisch, M., Döpelheuer, A., Gottschaldt, K., Baumann, R., Zöger, M., Sölch, I., Rautenhaus, M., and Dörnbrack, A.: In-situ observations of young contrails – overview and selected results from the CONCERT campaign, Atmos. Chem. Phys., 10, 9039–9056, doi:10.5194/acp-10-9039-2010, 2010.

Voigt, C., Schumann, U., Jessberger, P., Jurkat, T., Petzold, A., Gayet, J.-F., Krämer, M., Thornberry, T., and Fahey, D. W.: Extinction and optical depths from contrails, Geophys. Res. Lett., 38, L11806, doi:10.1029/2011GL047189, 2011.

Ziereis, H., Schlager, H., Schulte, P., van Velthoven, P. F. J., and Slemr, F.: Distributions of NO, NO_x, and NO_y in the upper troposphere and lower stratosphere between 28_ and 61_N during POLINAT 2, J. Geophys. Res., 105, 3653–3664, doi:10.1029/1999JD900870, 2000.

Zöger, M., Afchine, A., Eicke, N., Gerhards, M.-T., Klein, E., McKenna, D., Mörschel, U., Schmidt, U., Tan, V., Tuitjer, F., Woyke, T., and Schiller, C.: Fast in situ stratospheric hygrometers: A new family of balloon-borne and airborne Lymanphotofragment fluorescence hygrometers., J. Geophys. Res., 104, 1807–1816, doi:10.1029/1998JD100025, 1999.

ACPD
11, 26867–26895, 2011

Table 1. Mean values of parameters over the indicated time-intervals and corresponding contrail ages for the three selected contrail regions A, B and C (see Fig. 2). The parameters are: altitude, temperature, NO_y, concentration of particles ($d > 0.9\,\mu m$), effective diameter, ice water content, direct (PN) and retrieved extinction coefficients (Ext and Ext R, respectively), asymmetry parameter, spherical/aspherical partitioning ratio (SAR) and residual (Res).

#	Time (UT)	Age (s)	Alti. (m)	T (°C)	NO_y (nmol mol^{-1})	Conc (cm$_{-3}$)	D_{eff} (µm)	IWC (mg m^{-3})	Ext (km^{-1})	Ext R (km^{-1})	g	SAR (%)	Res. (%)
A	12:14:01 12:14:21	70	10 536	−54.5	17.1	219	3.5	4.7	3.50	2.77	0.873	100	13.6
B	12:16:44 12:17:05	105	10 640	−55.7	6.6	193	4.4	5.9	4.29	4.08	0.850	68	7.7
C	12:23:43 12:25:04	205	10 651	−56.8	8.5	63	4.8	1.9	1.08	1.15	0.805	44	9.7

ACPD
11, 26867–26895, 2011

Fig. 1. Picture taken from the Falcon cockpit a few minutes prior the penetration to the A380 contrail (from T. Jurkat).

ACPD
11, 26867–26895, 2011

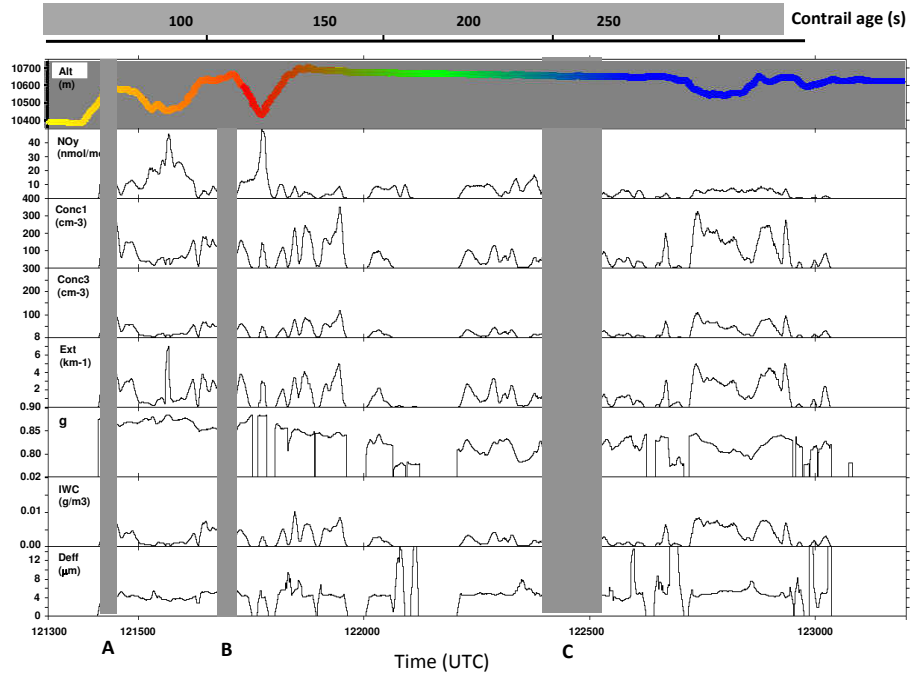

Fig. 2. Time-series (1 Hz) of the altitude and the NO_y measurements along with the concentrations of particles with diameter greater than 0.9 µm (Conc1) and greater than 2.5 µm (Conc3), the extinction coefficient (Ext), the asymmetry parameter (g), the ice water content (IWC) and the effective diameter (D_{eff}). The approximate time separation between the two aircraft is also reported indicating the A380 contrail age at the considered sampling time. The shaded colors of the altitude time-serie have been defined according to the contrail age. A, B and C shadowed zones refer to selected periods for the interpretation of retrieved results (see text, Sect. 4).

ACPD
11, 26867–26895, 2011

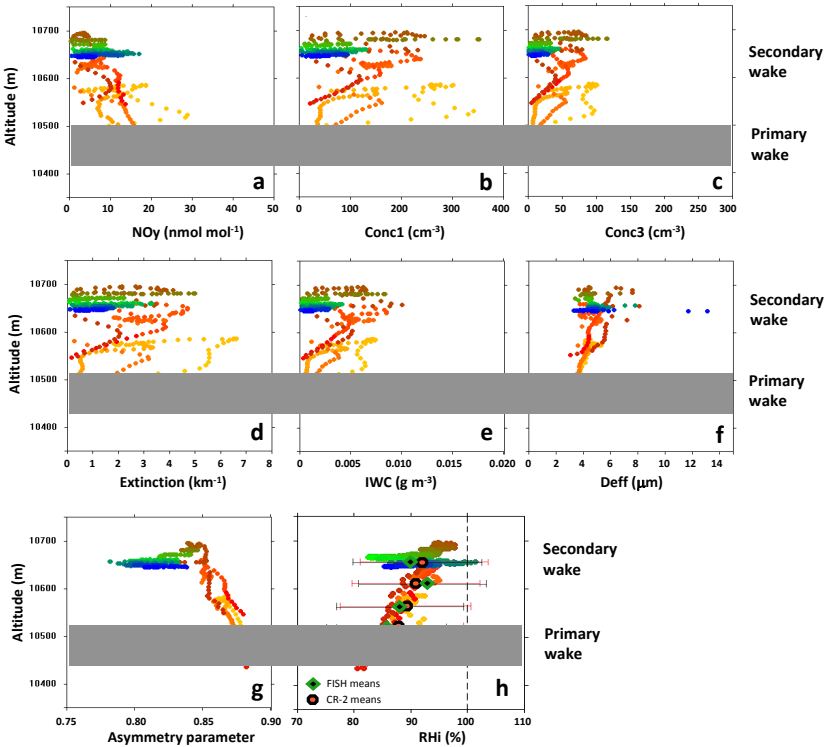

Fig. 3. Vertical distribution of parameters (1-s data) measured in the contrail from 12:14:00 UT to 12:26:00 UT (70–220 s contrail age, see Fig. 2). **(a)** NO_y mixing ratio, **(b)** concentration of particles $d > 0.9$ µm, **(c)** concentration of particles $d > 2.5$ µm, **(d)** exinction coefficient (PN), **(e)** ice water content, **(f)** effective diameter, **(g)** asymmetry parameter, and **(h)** relative humidity over ice. Mean FISH and CR-2 values are reported with error bars (±10 and ±12 %, respectively) which include systematic temperature and water vapor mixing ratio errors. The shaded colors of the altitude time-serie have been defined according to the contrail age (see Fig. 2).

ACPD
11, 26867–26895, 2011

The evolution of microphysical and optical properties

J.-F. Gayet et al.

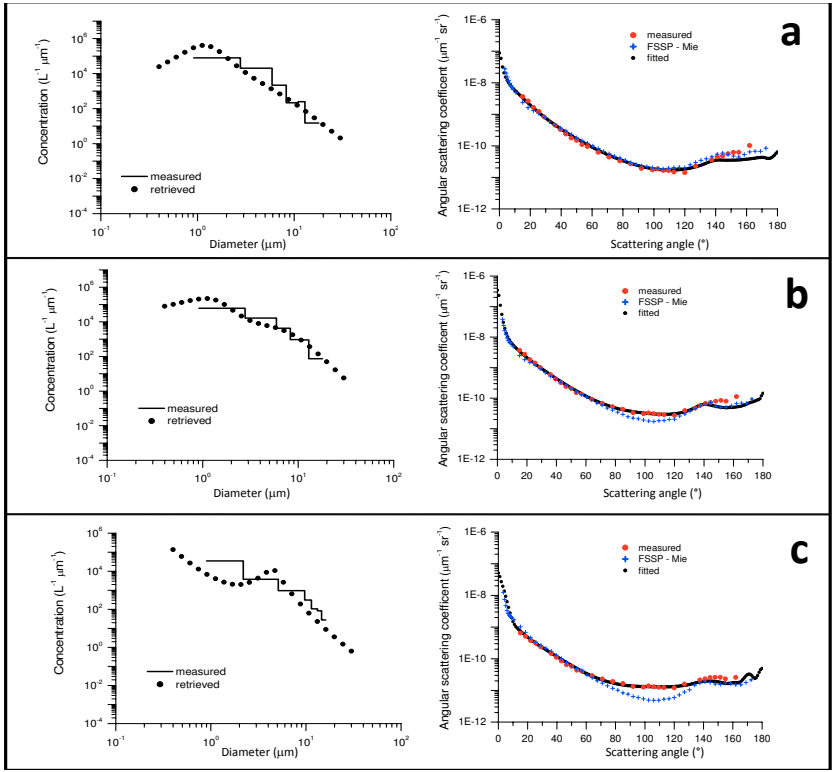

Fig. 4. Right panel: average scattering phase function (solid red circles), theoretical phase function (blue plus-symbols) calculated from the FSSP-300 size distribution (assuming spherical ice particles) and retrieved (solid black circles) scattering phase function. Left panel: direct particle size distribution (FSSP-300) and retrieved particle size distribution (solid black circles) from the measured scattering phase function. Cases A, B and C refer to the sampling at different contrail ages: 50 s, 105 s and 205 s, respectively.

ACPD
11, 26867–26895, 2011

The evolution of microphysical and optical properties

J.-F. Gayet et al.

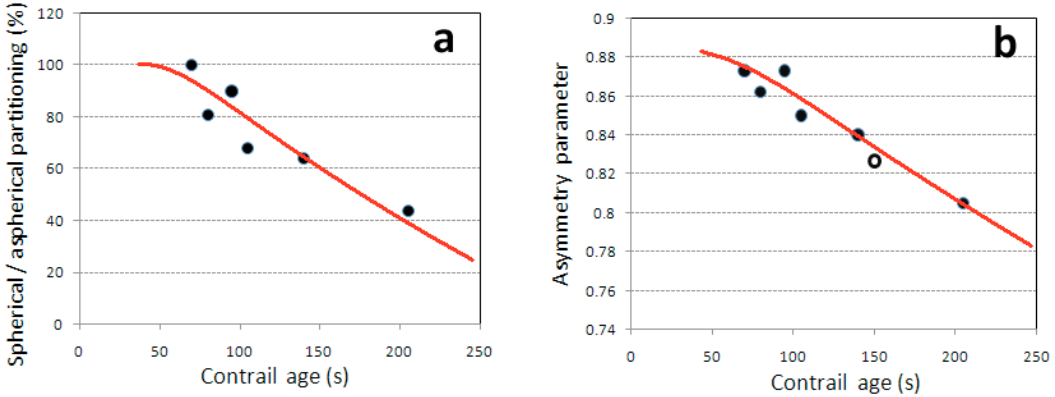

Fig. 5. Relationships between **(a)** the partitioning ratio (SAR) and **(b)** the asymmetry parameter versus the contrail age. The black dots represent experimental data and the red lines the approximate fits. The open circle corresponds to the Febvre et al.'s result (2009).

ACPD
11, 26867–26895, 2011